Lithuanian Journal of Physics, Vol. **47**, No. 3, pp. 279–288 (2007) doi:10.3952/lithjphys.47316

NUMERICAL TREATMENT OF THE TEMPERATURE DISTRIBUTION IN END-PUMPED COMPOSITE LASER RODS

A.S. Dement'ev [a], A. Jovaiša [a], K. Račkaitis [a], F. Ivanauskas [b], and J. Dabulytė-Bagdonavičienė [b]

[a] *Laboratory of Nonlinear Optics and Spectroscopy, Institute of Physics, Savanorių 231, LT-02300 Vilnius, Lithuania*
E-mail: aldement@ktl.mii.lt

[b] *Department of Computer Science, Vilnius University, Naugarduko 24, LT-03225 Vilnius, Lithuania*

Received 20 June 2007

Analytical and numerical studies of the thermal characteristics of conventional and composite laser rods in laser-diode end-pumped geometry are reported in detail using Nd : YAG rods as an example. It has been shown that taking into account the temperature dependence of the heat conductivity, the change of the temperature in the active element can be significantly higher compared to the data for the temperature-independent heat conductivity coefficient. It has been found that the dependence of heat conductivity on temperature causes the non-parabolic heat distribution even in the region inside the pump beam with the top hat intensity distribution. It has also been shown by direct numerical simulations that the undoped entrance section of the composite rod significantly reduces the peak temperature rise inside the crystal.

Keywords: diode-pump solid-state lasers, composite rod, thermal effects

PACS: 42.15.Eq, 42.55.Rz, 42.60.By, 44.10.+i

1. Introduction

Thermal effects play a very important role in solid-state lasers causing thermal distortion of the generated beam and limit the average power due to possible fracture of active elements by the induced thermal stresses. Therefore, these effects attract much attention and the results of previous investigation of this problem for lasers with the edge lamp pumping are described in many monographs and textbooks [1–7]. A new stage of the investigations of the thermal effects started with the development of solid-state lasers with longitudinal pumping by laser diodes [6–12]. Laser-diode pumped solid-state lasers are nowadays covering a wide range of applications. High intensity pump beams are required to achieve sufficient inversion in the laser materials. However, part of the pump power is transformed into heat in a small volume inside the active media. In this case, a few new problems arise.

Firstly, the heat deposition is significantly inhomogeneous along the beam propagation axis. The analytical treatment of this thermal problem is rather complicated. The expression for temperature distribution obtained using the Dinis series (see [13–15] and refs. therein) is described by the infinite sum of cumbersome terms with Bessel functions, and is, therefore, inconvenient for practical applications. The approximate analytical solution of the heat transfer equation was obtained in [16] neglecting the longitudinal derivatives with respect to the radial derivatives. It has been shown that taking into account only the radial heat flow, for the cases considered, the obtained analytical solution agrees with the full numerical solution within 10% at the entrance face of the laser rod. It can be easily shown that for the common case with an air cooled end faces of the laser rod the end heat fluxes are small enough. Therefore, the problem for the mean (along the axial direction) temperature is identical to a two-dimensional problem of the radial heat flow [17]. Apparently that is not true for the case of the composite laser element where the heat transfer occurs through the additional edge surface of undoped part of the rod [18–20].

Secondly, the temperatures in the heated regions of the laser rod may be high enough. Therefore, the temperature dependence of the parameter of the active media should be taken into account [4, 21–25]. A few analytic solutions are known for the transversally pumped cylindrical laser rods with a parabolic pump profile only [21, 25].

Thirdly, anisotropy plays an important role in crystals

ISSN 1648-8504

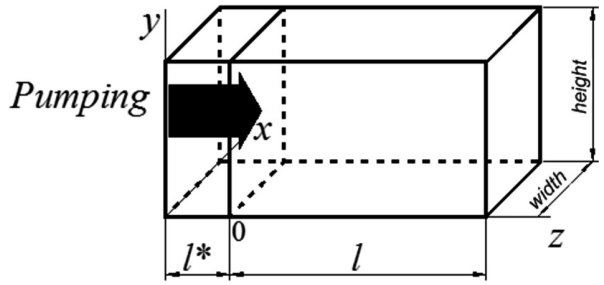

Fig. 1. Geometry of the end-pumped composite laser rod; l^* is the undoped crystal part and l is the Nd-doped part.

because the pump generated heat is distributed in the crystal non-homogenously in different directions corresponding to the crystallographic axis. All these problems are widely discussed in modern literature and recent overview articles, however, there are many factors that influence the heat production and distribution processes, and not enough attention is paid to them. It also should be evaluated how different boundary conditions, different shapes of active elements and cooling geometries, influence the temperature distribution. In this paper, the mathematical problem of the transient heat distribution is formulated, and afterwards, the influence of the pump beam geometry on the temperature distribution inside the rod is discussed. Then the algorithm used for numerical simulations is briefly presented, and, after that, the results of numerical modelling are compared with the known and original analytical solutions. Some final remarks are done in conclusions.

2. Mathematical model and algorithm

Since the active rods in longitudinally end-pumped solid-state lasers are recently used in the form of the rectangular parallelepiped, here we consider such a case (Fig. 1) of pumping and edge-cooled arrangement. The space-time evolution of the temperature $T(x,y,z,t)$ in a solid-state laser is governed by the heat conduction equation [26]:

$$\rho C_p \frac{\partial T}{\partial t} = \frac{\partial}{\partial x}\left(k_x(T)\frac{\partial T}{\partial x}\right) + \frac{\partial}{\partial y}\left(k_y(T)\frac{\partial T}{\partial y}\right) + \frac{\partial}{\partial z}\left(k_z(T)\frac{\partial T}{\partial z}\right) + Q(x,y,z,t)\,, \quad (1)$$

where $Q(x,y,z,t)$ is the heat generated per unit volume per unit time, ρ is the mass density, C_p is the crystal specific heat at constant pressure, $k_x(T)$, $k_y(T)$, $k_z(T)$ are the temperature-dependent heat conductivity coefficients along crystallographic axes.

The heat production area in the crystal is the area where the heat is generated as the energy difference between the pump and laser photons, the so-called quantum defect [6, 7]. The developed algorithm and software (see below) allow calculating the temperature distribution for any space-time dependence of the heat source $Q(x,y,z,t)$. In simulations we mainly used two types of the stationary heat source with super-Gaussian axially symmetric distribution

$$Q_1(x,y,z,t) = \begin{cases} 0\,, & -l^* \le z \le 0\,, \\ Q_{10}\cdot\exp\left\{-2\left[\dfrac{(x-x_c)^2}{w^2}+\dfrac{(y-y_c)^2}{w^2}\right]^q\right\}\times & \\ \quad\times\exp(-\alpha z)\,, & 0 \le z \le l \end{cases} \quad (2)$$

and the elliptic distribution

$$Q_2(x,y,z,t) = \begin{cases} 0\,, & -l^* \le z \le 0\,, \\ Q_{20}\cdot\exp\left[-2\left(\dfrac{x-x_c}{w_x}\right)^{2p}-2\left(\dfrac{y-y_c}{w_y}\right)^{2q}\right]\times & \\ \quad\times\exp(-\alpha z)\,, & 0 \le z \le l \end{cases} \quad (3)$$

Here p and q are the coefficients indicating order of the super-Gaussian pump beam. We assume that the length of the rod is smaller than the length of the pumping beam waist, and therefore the transverse distribution of the heat source is the same in different sections of the rod. The length of the undoped crystal part was $l^* = 0$ for the conventional active element and it was assumed to be about $l/4$ for the composite element. The values of maximal density of heat sources $Q_{10,20}$ depend on the power P of the pump beam, the fractional thermal loading η_h, and the linear absorption coefficient α. These values are expressed by formulas

$$Q_{10} = \frac{\alpha\eta_h P}{\pi w^2 \frac{1}{q}\left(\frac{1}{2}\right)^{1/q}\Gamma\left(\frac{1}{q}\right)}\,, \quad (4)$$

and

$$Q_{20} = \frac{pq\eta_h\alpha P}{w_x w_y \left(\frac{1}{2}\right)^{1/(2p)}\left(\frac{1}{2}\right)^{1/(2q)}\Gamma\left(\frac{1}{2p}\right)\Gamma\left(\frac{1}{2q}\right)}\,, \quad (5)$$

if we neglect the saturation of the pump beam absorption in the active element and the beam widths w or $w_{x,y}$

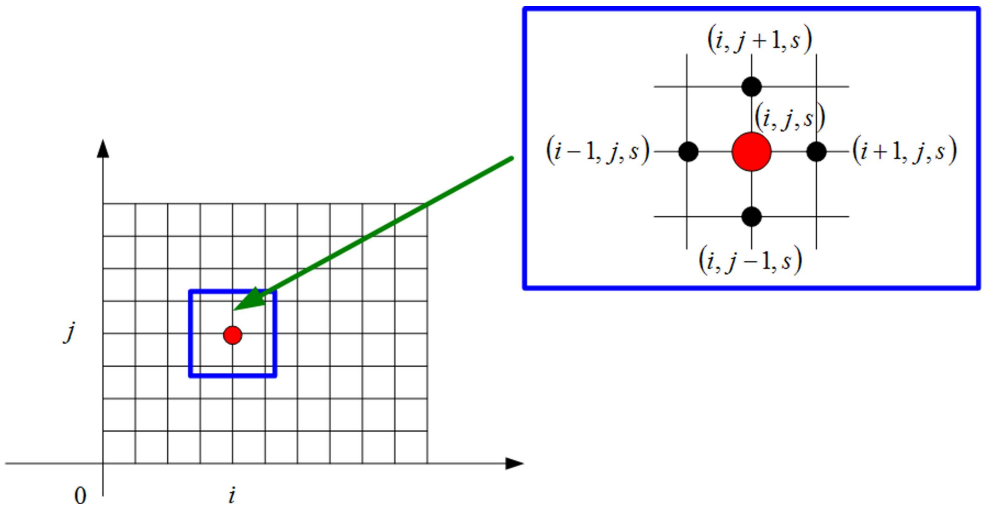

Fig. 2. Discretization mesh used in the numerical algorithm.

are much smaller than the distance from the axis of the beam to the edges of the rod. The fractional thermal loading η_h is defined as the ratio of the produced heat to the absorbed pump power. This coefficient was measured to be around 30% for Nd : YAG lasers pumped at 808 nm and about 10% for Yb : YAG lasers pumped at 943 nm [7]. If the order of the super-Gaussian beam is $q \gg 1$, then the distribution tends to be similar to the so-called top hat distribution with the radius w. But for the same pump power and the same maximal heat generation density as for the common Gaussian beam ($q = 1$), the radius of the top hat beam should be $r_0 = w/\sqrt{2}$.

After describing the main equation, which is governing the temperature distribution inside the laser crystal, initial and boundary conditions have to be established. The initial condition specifies temperature distribution in the medium at the initial time coordinate $T(x, y, z, 0) = T_a(x, y, z)$, which depends on the ambient surroundings.

The boundary conditions specify the heat flow on the boundaries of the rod and they are given by the Newton's law of the heat transfer [26]:

$$\begin{aligned} \frac{\partial T}{\partial x} &= \frac{h_{x0}}{k_x(T|_{x=0})}(T|_{x=0} - T_a|_{x=0})\,, \\ \frac{\partial T}{\partial x} &= \frac{h_{xa}}{k_x(T|_{x=a})}(T_a|_{x=a} - T|_{x=a})\,, \end{aligned} \tag{6}$$

$$\begin{aligned} \frac{\partial T}{\partial y} &= \frac{h_{y0}}{k_y(T|_{y=0})}(T|_{y=0} - T_a|_{y=0})\,, \\ \frac{\partial T}{\partial y} &= \frac{h_{yb}}{k_y(T|_{y=b})}(T_a|_{y=b} - T|_{y=b})\,, \end{aligned} \tag{7}$$

$$\begin{aligned} \frac{\partial T}{\partial z} &= \frac{h_{z(-l^*)}}{k_z(T|_{z=-l^*})}(T|_{z=-l^*} - T_a|_{z=-l^*})\,, \\ \frac{\partial T}{\partial z} &= \frac{h_{zl}}{k_z(T|_{z=l})}(T_a|_{z=l} - T|_{z=l})\,. \end{aligned} \tag{8}$$

Here the possibility to set different heat transfer coefficients $h_{x,y,z}$ and cooling temperatures $T_a|_{x,y,z}$ at different crystal walls is taken into account. It should also be noted that the heat flows on different crystal edges depend on the rod temperature on these edges $T|_{x,y,z}$.

YAG crystal parameters were used in our calculations because the physical properties of this crystal are most widely explored experimentally [3, 7]. It is known that thermal parameters of the doped YAG depend on the concentration of the doped ions [7]. It is especially significant for the Yb-doped YAG crystal because the thermal conductivity for the 10% doped crystal can decrease more than twice compared to the Nd-doped crystal. The concentration of Nd ions cannot be so high in the YAG crystal and we here neglect the possible dependence of thermal conductivity on the Nd concentration.

The thermal conductivity is temperature-dependent, and around 300 K this coefficient is described well by the following formula [25]:

$$k_1(T) = k_0\left(\frac{T_0}{T}\right)^{\zeta}, \quad T_0 = 300\ \mathrm{K}\,. \tag{9}$$

The case $\zeta = 0$ is that of the constant conductivity, the case $\zeta = 1$, i. e., $k_1(T) = k_0 T_0/T$, was used in [4, 21]. It is claimed in [25] that at around 300 K the experimental values are best described by $\zeta = 0.7$.

A more complicated fitting procedure for experimen-

tal data of Nd : YAG was used in [23, 24] where the following expression was derived:

$$k_2(T) = \frac{a}{\left[\ln(bT)\right]^c} - \frac{d}{T}, \qquad (10)$$

here $a = 1.9{\cdot}10^6$ W/(cm K), $b = 5.33$ 1/K, $c = 7.14$, $d = 331$ W/cm.

The finite difference technique and its explicit scheme were used for the discretization of the mathematical model [27, 28]. Here we will only briefly describe discretization of the studied crystal block shown in Fig. 2. Temperature in the numerical model can be described by the equation $T(x, y, z, t) = T(x_i, y_j, z_s, t_n) = T(i, j, s, n) = T^n_{ijs}$. Then the constructed discrete mesh shown in Fig. 2 for the laser crystal block is described as

$$x_i = i \cdot h_1, \quad i = \overline{0, N_1}, \quad h_1 = \frac{x_1}{N_1}, \qquad (11)$$

$$y_j = j \cdot h_2, \quad j = \overline{0, N_2}, \quad h_2 = \frac{y_1}{N_2}, \qquad (12)$$

$$z_s = s \cdot h_3, \quad s = \overline{0, N_3}, \quad h_3 = \frac{z_1}{N_3}, \qquad (13)$$

$$t_n = n \cdot \tau, \quad n = \overline{0, M}. \qquad (14)$$

Time step τ was chosen to satisfy the solution stability condition $\tau \le h^2/(6D)$, here $h = \min\{h_1, h_2, h_3\}$ and $D = \max\{D_1, D_2, D_3\}$, where $D_i = k_i(T_0)/(\rho C_p)$ are thermal diffusion coefficients; h_1, h_2, h_3 are steps of spatial coordinates, N_1, N_2, N_3 are the numbers of intervals in respective directions of dimensions x_1, y_1, z_1 of the rod.

Let us now consider the used approximation of differential equation (1) and initial and boundary conditions (Eqs. (6)–(8)) by difference equations. After approximation of heat conductivity Eq. (1) we have a set of difference equations:

$$T^{n+1}_{ijs} = \frac{\tau}{\rho C_p}\left[\frac{k_x(T^n_{i+1,j,s})T^n_{i+1,j,s}}{h_1^2} + \frac{k_x(T^n_{i,,j,s})T^n_{i-1,j,s}}{h_1^2} + \frac{k_y(T^n_{i,j+1,s})T^n_{i,j+1,s}}{h_2^2} + \frac{k_y(T^n_{i,,j,s})T^n_{i,j-1,s}}{h_2^2} + \frac{k_z(T^n_{i,j,s+1})T^n_{i,j,s+1}}{h_3^2} + \frac{k_z(T^n_{i,,j,s})T^n_{i,j,s-1}}{h_3^2}\right.$$

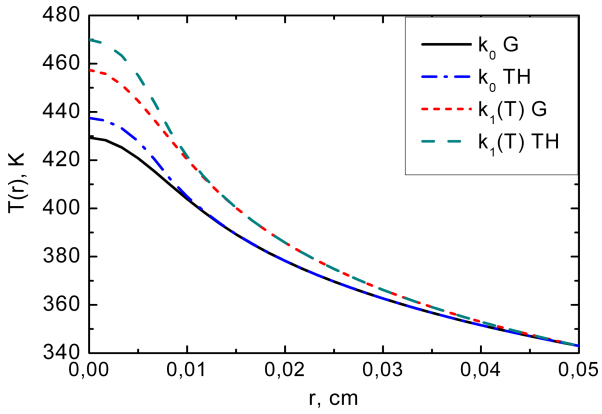

Fig. 3. Analytically calculated radial temperature profiles for the cylindrical active element. Gaussian (G) and top hat (TH) pumping profiles were used for constant ($k_0 = 0.13$ W/(cm K)) and temperature-dependent ($k_1(T) = a/T$, where $a = 39$ W/cm) heat conductivity coefficients. Gaussian pump profile radius was $w = 0.01$ cm, top hat $r_0 = 7.07{\cdot}10^{-3}$ cm.

$$\left. - \left(\frac{1}{h_1^2}k_x(T^n_{i,j,s}) + \frac{1}{h_2^2}k_y(T^n_{i,j,s}) + \frac{1}{h_3^2}k_z(T^n_{i,j,s}) - \frac{\rho C_p}{\tau}\right) \cdot T^n_{ijs} + Q_{0ijs}\right], \qquad (15)$$

where $i = \overline{1, N_1 - 1}$, $j = \overline{1, N_2 - 1}$, $s = \overline{1, N_3 - 1}$. After approximation of initial conditions by finite difference, we get

$$T^0_{ijs} = T_a, \qquad (16)$$

where $i = \overline{0, N_1}$, $j = \overline{0, N_2}$, $s = \overline{0, N_3}$.

Using this algorithm the original software that allows simulating different cases of the laser rod heating by the continuous pumping with different space distributions of the pump power was developed.

3. Results and discussion

Before presenting the results of numerical simulation, we discuss a more simple steady-state heat flow in isotropic cylindrical rods with radially symmetric heating distributions. In this case Eq. (1) can be written as

$$\frac{1}{r}\frac{\partial}{\partial r}\left(k(T) r \frac{\partial T}{\partial r}\right) + \frac{\partial^2 T}{\partial z^2} = -Q(r, z). \qquad (17)$$

Neglecting the longitudinal (i. e., z) derivatives with respect to the radial derivatives, i. e., assuming only the radial heat flow, the dependence on the longitudinal coordinate z is included in an analytical solution through

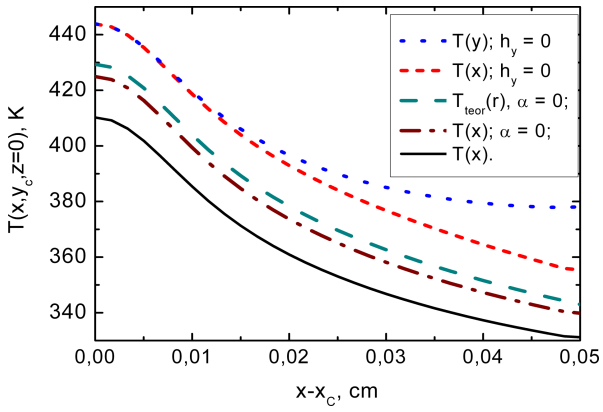

Fig. 4. Temperature profiles along the active element radius, for Gaussian pumping $w = 0.01$ cm for different cases: numerical data for the rectangular active element cooled from all four sides, $\alpha z \neq 0$ (solid line) and without cooling and $\alpha z = 0$ (dashed line); analytically calculated temperature profile for the cylindrical rod without cooling and $\alpha z = 0$ (dash dotted line); numerically calculated temperature profiles for the active element cooled only from two sides – along x (short dashed line) and y (dotted line) axes. Heat conductivity was set to $k = 0.13$ W/(cm K), the heat transfer coefficient of cooled surfaces was $h = 2$ W/cm^{2}K.

the heat source as an external parameter [16, 17]. In this case Eq. (17) becomes simpler:

$$\frac{1}{r}\frac{\partial}{\partial r}\left(k(T) r \frac{\partial T}{\partial r}\right) = -Q(r)\,, \tag{18}$$

where dropped z-dependence is also in $Q(r, z)$. For the case of the constant thermal conductivity, solutions of Eq. (18) for top hat (TH) and Gaussian (G) transverse pump power distributions are known [16, 29]. The general solution of Eq. (18) for the constant thermal conductivity with an arbitrary axially symmetric heating distribution was obtained in [30]. Unfortunately, this solution is rather cumbersome and the explicit solution for a given distribution of the heat source with the help of this solution is not easily obtained. Therefore, we also demonstrate the differential method, which allows obtaining the explicit solutions for temperature-dependent thermal conductivity of the rod.

For the top hat pump beam, Eq. (18) can be written in the form of two equations:

$$\frac{1}{r}\frac{\mathrm{d}}{\mathrm{d}r}\left(k_0 r \frac{\mathrm{d}T}{\mathrm{d}r}\right) = -Q_0\,, \quad 0 \le r \le r_0\,, \tag{19}$$

$$\frac{1}{r}\frac{\mathrm{d}}{\mathrm{d}r}\left(k_0 r \frac{\mathrm{d}T}{\mathrm{d}r}\right) = 0, \quad r_0 < r \le R\,, \tag{20}$$

where r_0 is the radius of the beam and R is the radius of the rod. Integrating these equations and using boundary conditions

$$-k_0 \frac{\mathrm{d}T}{\mathrm{d}r}(r_0^-) = -k_0 \frac{\mathrm{d}T}{\mathrm{d}r}(r_0^+),\; T(r_0^-) = T(r_0^+)\,, \tag{21}$$

it is easy to obtain the known solution [29]

$$T(r) = T_a + \frac{Q_0 r_0^2}{2hR_0} + \frac{Q_0 r_0^2}{4k_0} \times$$

$$\times \begin{cases} 1 - (r/r_0)^2 + 2\ln\dfrac{R_0}{r_0}\,, & 0 \le r \le r_0\,, \\ -2\ln\dfrac{r}{R_0}\,, & r_0 < r \le R_0\,. \end{cases} \tag{22}$$

Introducing the dimensionless value $q_0 = Q_0 r_0^2/(2k_0 T_0)$, the solution of Eq. (22) in the region $0 \le r \le r_0$ can be written as

$$T(r) = T_{C1} - \frac{q_0 T_0}{2}\frac{r^2}{r_0^2}\,, \tag{23}$$

where

$$T_{C1} = T_a + \frac{Q_0 r_0^2}{2hR_0} + \frac{Q_0 r_0^2}{4k_0} + \frac{Q_0 r_0^2}{2k_0}\ln\frac{R_0}{r_0}\,. \tag{24}$$

For the Gaussian beam with the heat source in the form $Q(r) = Q_0 \exp\left[-2(r/w)^2\right]$, the solution of Eq. (18) can be written as

$$T(r) = T_{C2} - q_w T_0 \overline{T}(r)\,, \tag{25}$$

$$T_{C2} = T_a + q_w T_0 \frac{k_0}{hR_0}\left[1 - \exp(-2R_0^2/w^2)\right]$$

$$+ q_w T_0 \overline{T}(R_0)\,, \tag{26}$$

$$\overline{T}(r) = \int_0^{\sqrt{2r/w}} \left[1 - \exp(-\rho^2)\right]\frac{\mathrm{d}\rho}{\rho}\,,\; q_w = \frac{Q_0 w^2}{4k_0 T_0}\,. \tag{27}$$

In [16] the solution of Eqs. (26), (27) is expressed via the exponential integral function. Using standard commercial mathematical programs such as Mathcad, it is simpler to calculate the integral (Eqs. (26), (27)) directly. For the points near the beam axis ($r \ll w$), the solution of Eq. (25) can be written in the form

$$T(r) \approx T_{C2} - q_0 T_0 \left(\frac{r^2}{r_0^2} - 3\frac{r^4}{r_0^4}\right)\,, \tag{28}$$

where for a more convenient comparison with the top hat solution the same notation ($r_0 = w/\sqrt{2}$) is used for the same pump power and the same maximal heating density Q. It can be seen from Eqs. (23) and (28) that

a Gaussian pump beam leads to the spherically aberrated thermal lens with a twice smaller focal length as compared to the top hat beam with the same power dissipation and slightly smaller spot radius $r_0 = w/\sqrt{2}$ (not the same as claimed in [9]).

Two different steady-state temperature distribution profiles are known in the case of the temperature-dependent thermal conductivity (Eq. (9)) for a parabolic pump profile: (i) for $\zeta = 1$ [4, 21] and (ii) for $\zeta \neq 1$ [25]. We will present new solutions for the case $\zeta = 1$ for the pump beam with top hat and Gaussian profiles. Using the same differential method it is not difficult to obtain the following solution of Eq. (18) for the top hat pumping beam:

$$T(r) = T_{C3}\,\exp\left[-\frac{q_0}{2}\left(\frac{r^2}{r_0^2}\right)\right],\ 0 \le r \le r_0\,, \qquad (29)$$

$$T(r) = \left[\frac{q_0 k_0 T_0}{hR_0} + T_a\right]\left(\frac{R_0}{r}\right)^{q_0},\ r_0 < r \le R_0\,. \qquad (30)$$

Here $T_{C3} = [q_0 k_0 T_0/(hR_0) + T_a]\,\mathrm{e}^{q_0/2}\,(R_0/r_0)^{q_0}$ is the temperature at the pump beam axis. The expansion of the exponential for the case of $0 \le r \ll r_0$ and neglecting terms with the power higher than 4 leads to the expression

$$T(r) = T_{C3}\left[1 - \frac{q_0}{2}\frac{r^2}{r_0^2} - \frac{q_0^2}{8}\frac{r^4}{r_0^4}\right]. \qquad (31)$$

It is easy to find that $T_{C1} < T_{C3}$. Therefore, in the case of the temperature-dependent thermal conductivity, the induced thermal lens is spherically aberrated even for the top hat pump beam and has a shorter focal length.

For a Gaussian pump beam, the analogous expressions can be easily obtained:

$$T(r) = T_{C4}\exp\left[-q_w\overline{T}(r)\right], \qquad (32)$$

$$T_{C4} = \left\{T_a + q_w T_0\frac{k_0}{hR_0}\left[1 - \exp\left(\frac{-2R_0^2}{w^2}\right)\right]\right\} \times \exp\left[q_w\overline{T}(R_0)\right]. \qquad (33)$$

Near the axis of the pump beam, the following formula for temperature distribution can be obtained:

$$T(r) \approx T_{C4}\left[1 - q_w\overline{T}(r) + \frac{q_w^2\overline{T}^2(r)}{2}\right] \approx \approx T_{C4}\left[1 - q_w\frac{r^2}{r_0^2} + \left(3q_w + \frac{q_w^2}{2}\right)\frac{r^4}{r_0^4}\right]. \qquad (34)$$

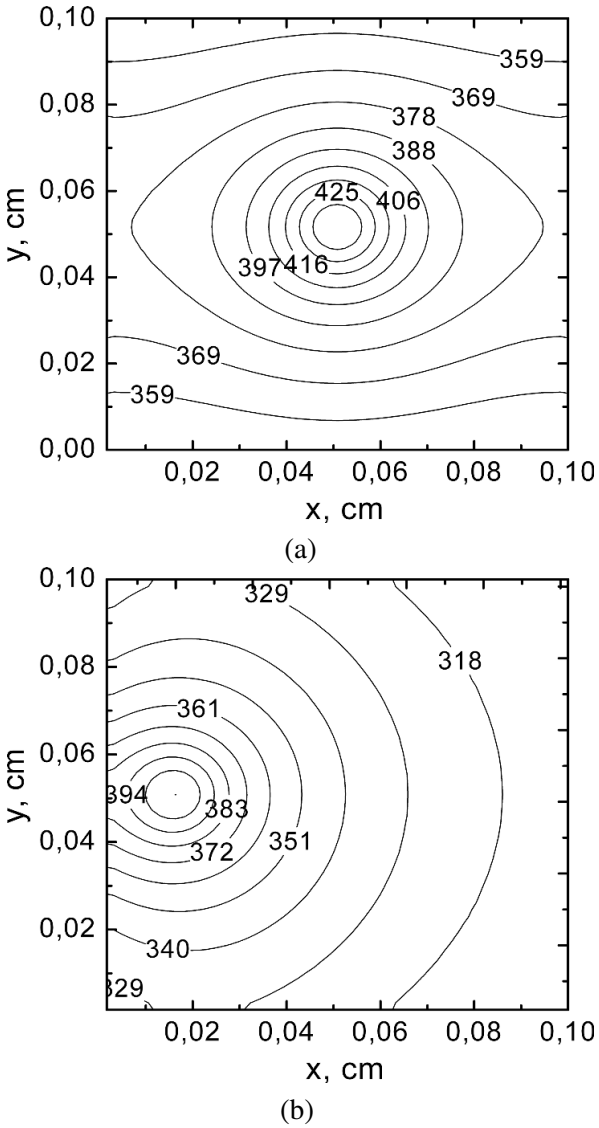

Fig. 5. Contour lines for the temperature profiles at $z = 0$ plane, for different active element cooling settings (a) when only two side walls were properly cooled with the heat transfer coefficient $h = 2$ W/(cm^{2}K) and (b) when all four side walls were cooled, but the pumping area was shifted closer to one side. Heat conductivity was set to $k = 0.13$ W/(cm K), Gaussian pumping $w = 0.01$ cm.

Figure 3 illustrates analytically calculated temperature profiles for cylindrical active elements (AE) pumped by Gaussian (G) and top hat (TH) beams, using Eqs. (23)–(25), (29), (30), (32), (33). In calculations the following parameter values of AE were used: $k_0 = 0.13$ W/(cm K), $T_0 = 300$ K, $T_a = 293$ K, $R_0 = 0.05$ cm, $w = 0.01$ cm, $r_0 = 70.7$ μm, $Q_0 = 2{\cdot}10^5$ W/cm^3, $h = 2$ W/(cm^{2}K). The same AE parameters were also used in other numerical simulations unless other values were indicated additionally.

From calculations it can be seen that the maximum temperature at the centre of the crystal rod is as follows: $T_{C2} < T_{C1} < T_{C4} < T_{C3}$. It can be seen from Fig. 3

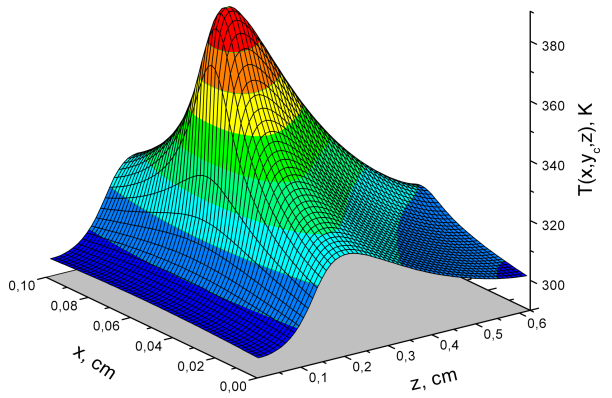

Fig. 6. 3D temperature profile for the composite active element with Gaussian pumping $w = 0.01$ cm; heat conductivity was set to $k = 0.13$ W/(cm K), the heat transfer coefficient $h = 2$ W/(cm^{2}K).

that the temperature distributions for Gaussian and top hat beams strongly differ only in the inner region of pump beams ($r \leq w$). The temperature distributions practically coincide in the outer region of the beams inside the rod, though analytical expressions for temperature distribution are very different. It should also be noted that signs of Taylor series terms are the same for the top hat pump beam (see Eqs. (23), (24), (31)) and different for the Gaussian beam (Eqs. (28) and (34)). Therefore, in the region $r \sim r_0$, the temperature gradient for the Gaussian beam is smaller than for the top hat pump beam.

Most of the numerical calculations were performed for the rectangular Nd : YAG active element with $1\times1\times5$ mm^3 dimensions for the conventional element and $1\times1\times6.25$ mm^3 for the composite element with the 1.25 mm long undoped entrance part of the element (Fig. 1). At first, we present the results (Fig. 4), which depict the influence of different cooling arrangements for the conventional Nd : YAG element with Gaussian pumping. The pump beam was assumed to have the waist radius $w = 0.1$ mm. The incident pump-generated heat with the maximal density is $Q_0 = 2{\cdot}10^5$ W/cm^3. The lowest maximal temperature (Fig. 4, solid line) is realized near the entrance face ($z = 0$) for the case of all cooled surfaces of AE: the side walls are water-cooled with the surface heat transfer coefficient $h_x = h_y = 2$ W/(cm^{2}K), the entrance and rear faces of AE are air-cooled with $h_z = 0.1$ W/(cm^{2}K). The temperature is notably higher (Fig. 4, dash dot line) for homogeneous heating along the z axis ($\alpha = 0$). The temperature for the cylindrical rod with the side surface water cooling ($h = 2$ W/(cm^{2}K), $h_z = 0$) and homogeneous ($\alpha = 0$) heating along the z axis (this case corresponds to the analytical result, depicted in Fig. 3 by solid line, for the constant thermal conductivity) is also slightly higher (Fig. 4, dash line) than for the rectangular rod (Fig. 4, dash dot line), when all side surfaces are cooled, because the coolant surface is larger in the latter case. If only two opposite sides of the rectangular rod are cooled, the temperature rises again visibly, but its distribution in the region $0 \leq r = \sqrt{x^2 + y^2} < w$ is practically the same in different directions (Fig. 4, short dash and dot lines).

This observation holds true not only for the centred pump beam (Fig. 5(a)), but also for the shifted pump beam and AE cooled from all sides (Fig. 5(b)). It is well seen that the isolines of constant temperature are concentric cycles. Thus, it can be concluded that positioning of the pump beam is not so critical for rods with the large enough transversal cross-section compared with the pump beam cross-section.

The 2D temperature profile for the composite laser rod is shown in Fig. 6. It is seen that for 1.25 mm long undoped part of YAG the increase in temperature at the entrance face is very small. Therefore, there is no need to use longer undoped entrance ends. The decrease in temperature inside the active medium is significant as compared to the conventional rod (Fig. 7(a, b)). It is seen that the temperature at the entrance face of the active medium decreases strongly, but at the exit face it practically does not change. The increase in temperature due to the temperature-dependent heat conductivity is also slightly diminished in the composite rod.

For the quasi three-level system such as Yb : YAG, the temperature increase should be small enough because it can strongly populate the lower working level of Yb ion. Therefore, in such media the temperature rise must be controlled carefully. If the temperature increase does not significantly disturb the population of the lower working level of active media as is the case with Nd : YAG, the other effects can limit the performance of the laser. The most significant of these effects is a thermally induced change of the optical path difference (OPD). It is commonly assumed that the optical path difference is essentially proportional to the temperature rise ΔT and can be found using formula

$$\mathrm{OPD} = \int \frac{\mathrm{d}n}{\mathrm{d}T}\,\Delta T\,\mathrm{d}z\,. \tag{35}$$

Here we will not specify the thermo-optic parameter $\mathrm{d}n/\mathrm{d}T$ exactly. In the calculation results presented below we use the common value of $\mathrm{d}n/\mathrm{d}T$ for Nd : YAG elements [7] and do not take into account its temperature dependence [23, 24]. The calculated OPD in the plane $y = y_C$ is presented in Fig. 8. It is seen that the calculated absolute changes of OPD/λ

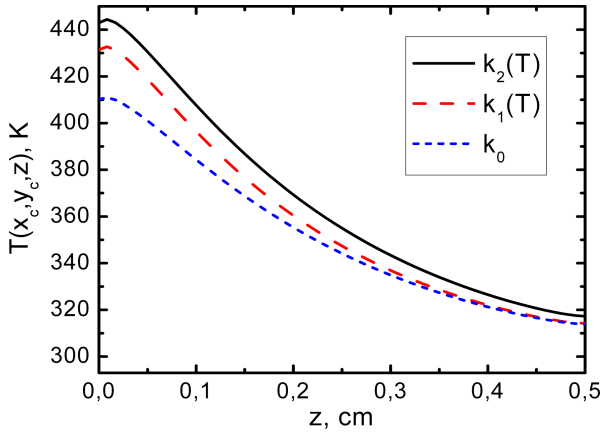

(a)

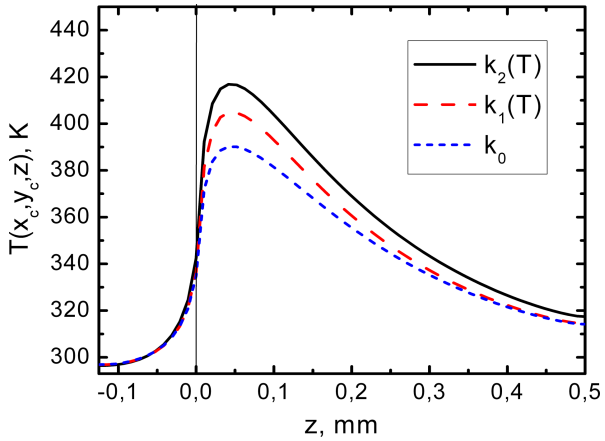

(b)

Fig. 7. Temperature at the centre of the active element along z axis for conventional and composite rods, with temperature-dependent heat conductivity coefficients (solid and dashed lines), calculated using Eqs. (9), (10) and the constant heat conductivity coefficient $k = 0.13$ W/(cm K) (dotted line). All calculations were performed for Gaussian pumping with radius $w = 0.01$ cm and for usual cooling heat transfer coefficient $h = 2$ W/(cm^{2}K).

in the conventional rod are more significant for both cases of the temperature-independent and temperature-dependent heat conductivity. Therefore, the use of composite rods can reduce the thermal lensing effect. This reduction can be more expressed for lasers with a longer active medium than in the case of very short ($\sim$1 mm) doped parts of AE [18, 19].

Our developed software makes it possible to set arbitrary heat conductivity coefficients along different axis in the crystal block. In this case, the distribution of temperature is different along the x and y axes. Therefore, the thermally induced lens is astigmatic in this case. The astigmatism of the thermal lens can be reduced using the elliptical pump beam. On the one hand, such variations in the pump beam shape and different crystal configurations can help diminish the maximum temperature in the crystal, although, on the other hand, astigmatism occurs in the crystal block. The use of our program allows us to optimize experimental arrangement of the laser oscillator or the amplifier and to improve performance of the constructed laser system.

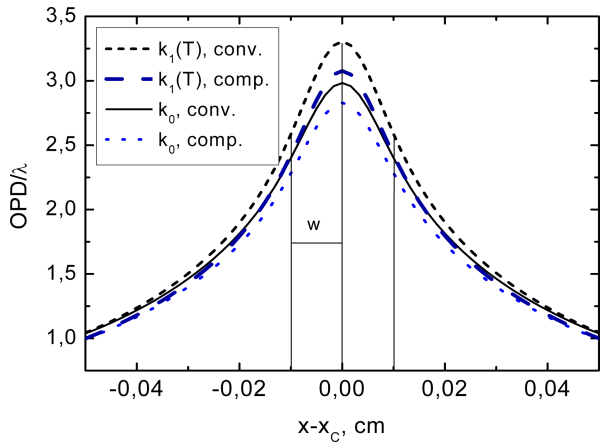

Fig. 8. Comparison of the numerically calculated optical path difference with constant ($k = 0.13$ W/(cm K)) and temperature-dependent ($k_1(T) = a/T$, where $a = 39$ W/cm) heat conductivity coefficients for conventional (solid and short dashed lines) and composite (dashed and dotted lines) active elements.

4. Conclusions

Analytical and numerical studies of the thermal characteristics for conventional and composite laser rods in laser-diode end-pumped geometry are reported in detail using Nd : YAG rods as an example. Using analytical solutions and numerical simulations conducted by the developed software, it has been shown that, when taking into account the temperature dependence of the heat conductivity, the temperature in the active element can be significantly higher compared with the data for the temperature-independent heat conductivity coefficient. This change in temperature is significant and should be taken into account when developing laser systems. The dependence of heat conductivity on temperature causes the non-parabolic heat distribution even in the region of the pump beam with the top hat intensity distribution. This leads to much more strongly spherically aberrated thermal lens and increases the wavefront distortion for both Gaussian and top hat pump beams. It is shown by direct numerical simulations that the undoped entrance section of the composite rod acts as an additional effective heat diffuser and significantly reduces the peak temperature rise inside the crystal. The thermally induced spherical aberration strongly complicates the laser beam distortion compensation. It has been shown that thermal lensing can be improved us-

ing composite laser rods with the undoped entrance end section.

Acknowledgement

This work has been partially supported by the Agency for International Science and Technology Development Programmes in Lithuania within the framework of the EUREKA project E!3483 EULASNET LASCAN.

References

[1] B.R. Belostockii and A.S. Rubanov, *Thermal Regime of Solid State Optical Quantum Generators* (Energiya, Moscow, 1973) [in Russian].

[2] A.V. Mezenov, L.N. Soms, and A.I. Stepanov, *Thermo-Optics of Solid-State Lasers* (Mashinostroenie, Leningrad, 1986) [in Russian].

[3] G.M. Zverev and Yu.D. Golyaev, *Crystal Lasers and their Application* (Radio i Svyaz, Moscow, 1994) [in Russian].

[4] N. Hodgson and H. Weber, *Optical Resonators. Fundamentals, Advanced Concepts and Applications* (Springer-Verlag, London, 1997).

[5] R. Ifflander, *Solid-State Lasers for Materials Processing* (Springer-Verlag, Berlin, 2001).

[6] W. Koechner and M. Bass, *Solid-State Lasers: A Graduate Text* (Springer-Verlag, New York, 2003).

[7] W. Koechner, *Solid-State Laser Engineering*, 6th ed. (Springer-Verlag, New York, 2006).

[8] R. Weber, B. Neuenschwander, and H.P. Weber, Thermal effects in solid-state laser materials, Opt. Mater. **11**(2–3), 245–254 (1999).

[9] W.A. Clarkson, Thermal effects and their mitigation in end-pumped solid-state lasers, J. Phys. D **34**(16), 2381–2395 (2001).

[10] S. Chenais, F. Balembois, F. Druon, G. Lucas-Leclin, and P. Georges, Thermal lensing in diode-pumped ytterbium lasers, part I: Theoretical analysis and wavefront measurements, IEEE J. Quantum Electron. **40**(9), 1217–1234 (2004).

[11] S. Chenais, F. Balembois, F. Druon, G. Lucas-Leclin, and P. Georges, Thermal lensing in diode-pumped ytterbium lasers, part II: Evaluation of quantum efficiencies and thermo-optic coefficients, IEEE J. Quantum Electron. **40**(9), 1235–1243 (2004).

[12] S. Chenais, F. Druon, S. Forget, F. Balembois, and P. Georges, On thermal effects in solid-state lasers: The case of ytterbium-doped materials, Prog. Quantum Electron. **30**(4), 89–153 (2006).

[13] U.O. Farrukh, A.M. Buoncristiani, and C.E. Byvik, An analysis of the temperature distribution in finite solid-state laser rods, IEEE J. Quantum Electron. **24**(11), 2253–2263 (1988).

[14] B.A. Usievich, V.A. Sychugov, F. Pigeon, and A. Tishchenko, Analytical treatment of the thermal problem in axially pumped solid-state lasers, IEEE J. Quantum Electron. **37**(9), 1210–1214 (2001).

[15] R.G. Beausoleil, E.K. Gustafson, M.M. Fejer, E. D'Ambrosio, W. Kells, and J. Camp, Model of thermal wave-front distortion in interferometric gravitational-wave detectors. I. Thermal focusing, J. Opt. Soc. Am. B **20**(6), 1247–1268 (2003).

[16] M.E. Innocenzi, H.T. Yura, C.L. Fincher, and R.A. Fields, Thermal modeling of continuous-wave end-pumped solid-state lasers, Appl. Phys. Lett. **56**(19), 1831–1833 (1990).

[17] A.K. Cousins, Temperature and thermal stress scaling in finite-length end-pumped laser rods, IEEE J. Quantum Electron. **28**(4), 1057–1069 (1992).

[18] M. Tsunekane, N. Taguchi, T. Kasamatsu, and H. Inaba, Analytical and experimental studies on the characteristics of composite solid-state laser rods in diode-end-pumped geometry, IEEE J. Select. Topics Quantum Electron. **3**(1), 9–18 (1997).

[19] M. Tsunekane, N. Taguchi, and H. Inaba, Improvement of thermal effects in a diode-end-pumped, composite Tm : YAG rod with undoped ends, Appl. Opt. **38**(9), 1788–1791 (1999).

[20] Z. Xiong, Z.G. Li, N. Moore, W.L. Huang, and G.C. Lim, Detailed investigation of thermal effects in longitudinally diode-pumped Nd : YVO_4 lasers, IEEE J. Quantum Electron. **39**(8), 979–986 (2003).

[21] N. Hodgson and H. Weber, Influence of spherical aberration of the active medium on the performance of Nd : YAG lasers, IEEE J. Quantum Electron. **29**(9), 2497–2507 (1993).

[22] R. Buzelis, A. Dement'ev, J. Kosenko, E. Murauskas, R. Vaicekauskas, and F. Ivanauskas, Amplification efficiency and quality alteration of short pulses amplified in the Nd : YAG amplifier in the saturation mode, Lithuanian Phys. J. **38**(4), 289–301 (1998).

[23] D.C. Brown, Ultrahigh-average-power diode-pumped Nd : YAG and Yb : YAG lasers, IEEE J. Quantum Electron. **33**(5), 861–873 (1997).

[24] D.C. Brown, Nonlinear thermal distortion in YAG rod amplifiers, IEEE J. Quantum Electron. **34**(12), 2383–2392 (1998).

[25] A.M. Bonnefois, M. Gilbert, P.Y. Thro, and J.M. Weulersse, Thermal lensing and spherical aberration in high-power transversally pumped laser rods, Opt. Commun. **259**(1), 223–235 (2006).

[26] H.S. Carslaw and J.C. Jaeger, *Conduction of Heat in Solids*, 2nd ed. (Oxford University Press, UK, 1959).

[27] A.A. Samarskii and P.N. Vabishchevich, *Numerical Heat Transfer* (Editorial URSS, Moscow, 2003) [in Russian].

[28] H.D. Baehr and K. Stephan, *Heat and Mass Transfer*, 2nd ed. (Springe-Verlag, Berlin, 2006).

[29] A. Lucianetti, Th. Graf, R. Weber, and H.P. We-

ber, Thermo-optical properties of transversely pumped composite YAG rods with Nd-doped core, IEEE J. Quantum Electron. **36**(2), 220–227 (2000).
[30] M. Schmid, Th. Graf, and H.P. Weber, Analytical model of the temperature distribution and the thermally induced birefringence in laser rods with cylindrically symmetric heating, J. Opt. Soc. Am. B **17**(8), 1398–1404 (2000).

TEMPERATŪROS SKIRSTINIO IŠILGINIO KAUPINIMO KOMPOZITINIUOSE LAZERIO STRYPUOSE SKAITINIS TYRIMAS

A.S. Dementjev [a], A. Jovaiša [a], K. Račkaitis [a], F. Ivanauskas [b], J. Dabulytė-Bagdonavičienė [b]

[a] *Fizikos institutas, Vilnius, Lietuva*
[b] *Vilniaus universitetas, Vilnius, Lietuva*

Santrauka

Analitiškai bei skaitmeniškai modeliuojami šiluminiai reiškiniai išilgai kaupinamuose Nd : YAG lazerių paprastuose ir kompozitiniuose aktyviuosiuose elementuose. Naudojant sukurtą skaitinę modeliavimo programą, įmanoma stebėti temperatūros skirstinį įvairios formos aktyviuosiuose elementuose bei, esant įvairioms kraštinėms sąlygoms, galima parinkti skirtingas aušinimo temperatūras, šilumos pernašos koeficientus arba kaupinimo sritis. Parodyta, kad dėl šilumos laidumo koeficiento priklausomybės nuo temperatūros lazerio aktyviajame elemente blogiau perduodama šiluma ir temperatūra jame tampa aukštesnė nei lazerio kristale su nepriklausančiu nuo temperatūros šilumos laidumu. Pastebėta, kad, kaupinant lazerio pluoštu su stačiakampiu erdviniu intensyvumo pasiskirstymu, šilumos laidumo priklausomybė nuo temperatūros sukelia neparabolinį šilumos pasiskirstymą net ir kaupinamoje aktyviojo elemento srityje. Dėl to aktyviajame elemente susidaro stipriai aberuotas šiluminis lęšis, kuris blogina generuojamo arba stiprinamo lazerio pluošto kokybę. Tiesioginiu skaitiniu modeliavimu parodyta, kad priekinė kompozitinio elemento dalis be aktyviųjų jonų gali žymiai sumažinti aukščiausią temperatūrą jo centre.